Journal of the Mechanics and Physics of Solids 59 (2011) 1231–1250

Contents lists available at ScienceDirect

Journal of the Mechanics and Physics of Solids

journal homepage: www.elsevier.com/locate/jmps

Thermomechanical behavior of thermoset shape memory polymer programmed by cold-compression: Testing and constitutive modeling

Guoqiang Li [a,b,*], Wei Xu [a]

[a] Department of Mechanical Engineering, Louisiana State University, Baton Rouge, LA 70803, USA
[b] Department of Mechanical Engineering, Southern University, Baton Rouge, LA 70813, USA

ARTICLE INFO

Article history:
Received 20 August 2010
Received in revised form
3 January 2011
Accepted 1 March 2011
Available online 9 March 2011

Keywords:
Shape memory polymer
Programming
Cold-compression
Thermoviscoelasticity
Structural relaxation

ABSTRACT

Programming is a key process for thermally activated stress or strain recovery of shape memory polymers (SMPs). Typically, programming requires an initial heating above the glass transition temperature (T_g), subsequent cooling below T_g and removal of the applied load, in order to fix a temporary shape. This work adopted a new approach to program thermoset SMPs directly at temperatures well below T_g, which effectively simplified the shape fixing process. 1-D compression programming below T_g and free shape recovery of a thermoset SMP were experimentally investigated. Functional stability of the shape fixity under various environmental attacks was also experimentally evaluated. A mechanism-based thermoviscoelastic–thermoviscoplastic constitutive model incorporating structural and stress relaxation was then developed to predict the nonlinear shape memory behavior of the SMP trained below T_g. Comparison between the prediction and the experiment showed good agreement. The structure dependence of the thermomechanical behavior of the SMP was further discussed through a parametric study per the validated constitutive model. This study validates that programming by cold-compression is a viable alternative for thermally responsive thermoset SMPs.

1. Introduction

Shape memory polymers (SMPs), a booming member of the shape memory materials family, have become increasingly preferable due to their low cost, malleability, damage tolerance, and large ductility (Behl and Lendlein, 2007; Lendlein et al., 2005; Otsuka and Wayman, 1998; Nakayama, 1991). These advantages enable them to be active in various applications such as micro-biomedical components, aerospace deployable equipment and actuation devices (Tobushi et al., 1996; Liu et al., 2004; Yakacki et al., 2007). Lately, confined shape recovery of shape memory polymers has been used for repeatedly sealing/closing structural-length scale impact damages (Li and John, 2008; Nji and Li, 2010a; John and Li, 2010). Most recently, a biomimetic two-step self-healing scheme, close-then-heal (CTH), has been proposed by Li and Nettles (2010) and Xu and Li (2010), and further detailed by Li and Uppu (2010), for healing structural-length scale damage

* Corresponding author at: Department of Mechanical Engineering, Louisiana State University, Baton Rouge, LA 70803, USA. Tel.: +1 225 578 5302; fax: +1 225 578 5924.
E-mail address: guoli@me.lsu.edu (G. Li).

0022-5096/$ - see front matter © 2011 Elsevier Ltd. All rights reserved.
doi:10.1016/j.jmps.2011.03.001

autonomously, repeatedly, and molecularly. This concept has been experimentally validated by Nji and Li (2010b). It is envisioned that SMPs will have a foreseeable future in light-weight self-healing structures.

Thermally responsive shape memory polymer is not smart without programming. A most common programming cycle starts with a deformation of the SMP at a temperature above the glass transition temperature (T_g). While maintaining the shape (strain) or stress, the temperature is lowered below T_g. With the subsequent removal of the applied load, a temporary shape is created and fixed. This completes the typical three-step programming process. The original permanent shape can then be recovered upon reheating above T_g. The programming and shape recovery complete a thermomechanical cycle. However, for practical applications such as large structures, programming at very high temperature is not a trivial task because it is a lengthy, labor-intensive, and energy-consuming process. It is desired to develop new programming approaches and constitutive models to govern the corresponding thermomechanical behavior, which depends on understanding of the underlying shape memory mechanisms.

Several typical theories have been developed to explain such thermomechanical profiles. Earlier rheological models (Tobushi et al., 1997; Bhattacharyya and Tobushi, 2000) were capable of capturing the characteristic shape memory behavior of SMPs but with limited prediction capability due to the loss of the strain storage and release mechanisms. Later developments such as mesoscale model (Kafka, 2001, 2008) and molecular dynamic simulation (Diani and Gall, 2007) propelled the understanding to a rather detailed level. Recently, the phenomenological approach (Morshedian et al., 2005; Gall et al., 2005; Liu et al., 2006; Yakacki et al., 2007; Chen and Lagoudas, 2008a, 2008b; Qi et al., 2008; Xu and Li, 2010) emerges to be an effective tool to macroscopically investigate the thermomechanical mechanism of SMPs. The work by Liu et al. (2006) is a typical example of these various phenomenological models, which proposed a continuum mixture of a frozen and an active phase controlled by a sole temperature dependent first-order phase transition concept for the thermally activated SMPs. Although arguably treating the SMPs as a special elastic problem without consideration of the time dependence, the model reasonably captures the essential shape memory responses to the temperature event. However, the involvement of nonphysical parameters such as volume fraction of the frozen phase and stored strain resulted in a controversial nonphysical interpretation of the glass transition process. In order to address such issues, Nguyen et al. (2008) presented a revolutionary concept which attributes the shape memory effects to the structural and stress relaxation rather than the traditional phase transition hypothesis. They proposed that the dramatic change in the temperature dependence of the molecular chain mobility, which describes the ability for the polymer chain segments to rearrange locally to bring the macromolecular structure and stress response to equilibrium, underpins the thermally activated shape memory phenomena of SMPs. The fact that the structure relaxes instantaneously to equilibrium at temperature above T_g but responds sluggishly at temperature below T_g, suggests that cooling macroscopically freezes the structure in a nonequilibrium configuration below T_g, and thus allows the material to retain a temporary shape. Reheating to above T_g reduces the viscosity, restores the mobility and allows the structure to relax to its equilibrium configuration, which leads to shape recovery. As the temperature dependent phase transition assumption is abandoned, this theory implicitly indicates that acquiring the shape memory capacity may not necessarily require a temperature event.

We believe that, as long as a nonequilibrium configuration can be created and maintained, SMPs will gain the shape memory capability, regardless of the temperature at which the nonequilibrium configuration is created. Therefore, in this study, we adopted a different thermomechanical programming process for thermally activated thermosetting SMPs. Instead of the heating then cooling steps, the programming was conducted at a constant temperature which was well below the T_g of the SMP.

It is noted that cold-drawing programming of thermoplastic SMPs has been conducted by several researchers. Lendlein and Langer (2002) indicated that shape memory polymer (SMP) can be programmed by cold-drawing but did not give sufficient details. Ping et al. (2005) investigated a thermoplastic poly(ε-caprolactone) (PCL) polyurethane for medical applications. In this polymer, PCL was the soft segment and can be stretched (tensioned) to several hundred percents at room temperature (15–20 °C below the melting temperature of the PCL segment). They found that the cold-drawing programmed SMP had a good shape memory capability. Rabani et al. (2006) also investigated the shape memory functionality of two shape-memory polymers containing short aramid hard segments and poly(ε-caprolactone) (PCL) soft segments with cold-drawing programming. As compared to the study by Ping et al. (2005), the hard segment was different but with the same soft segment PCL. Wang et al. (2010) further studied the same SMP by Ping et al. (2005). They used FTIR to characterize the microstructure change during the cold-drawing programming and shape recovery. They found that in cold drawing programming, the amorphous PCL chains orient first at small extensions, whereas the hard segments and the crystalline PCL largely maintain their original state. When stretched further, the hard segments and the crystalline PCL chains start to align along the stretching direction and quickly reach a high degree of orientation; the hydrogen bonds between the urethane units along the stretching direction are weakened, and the PCL undergoes stress-induced disaggregation and recrystallization while maintaining its overall crystallinity. When the SMP recovers, the microstructure evolves by reversing the sequence of the microstructure change during programming. Zotzmann et al. (2010) emphasized that a key requirement for materials suitable for cold-drawing programming is their ability to be deformed by cold-drawing. Based on their discussion, it seems that SMP has an elongation at break as high as 20% is not suitable for cold-drawing programming.

In this study, a thermosetting SMP was programmed by cold-compression. We focused on cold-compression instead of cold-drawing because (1) compression programming is the key for the thermosetting SMP based composite to close or narrow macroscopic cracks during confined shape recovery (Li and Nettles, 2010; Li and Uppu, 2010; Nji and Li, 2010b)

and (2) the elongation at break is about 4% for this thermosetting SMP at temperature below T_g, which is not suitable for cold-drawing (tensioning) programming (Zotzmann et al., 2010). In this study, the SMP specimens were isothermally and uniaxially compressed to a certain strain level and then held for relaxation with strain maintained. It was found that a decent fixity ratio could be achieved efficiently with an adequate prestrain and a relaxation time period. The stability of the fixed temporary shape was then verified under various environmental attacks such as water immersion and ultraviolet light exposure. Subsequent free shape recovery tests proved that the permanent shape was also recoverable upon heating, similar to the specimens programmed using the traditional approach. A continuum finite deformation based thermo-viscoelastic–viscoplastic model was then developed to understand such a phenomenon. The concept presented by Nguyen et al. (2008) that the shape memory effect in nature is the transition between equilibrium and nonequilibrium configuration of the SMP structure was adopted and extended to the isothermal shape fixity process below T_g. The Narayanaswamy–Moynihan model (Narayanaswamy, 1971; Moynihan et al., 1976) was incorporated to represent the structure relaxation. Comparisons with experiments showed that the model could fairly well reproduce the general thermomechanical behavior of the thermoset SMP. Subsequent parametric studies were conducted to explore the shape memory responses to different stimuli and different programming temperatures per the validated constitutive model.

2. Experimental method

2.1. Raw materials, curing, and specimens preparation

The shape memory polymer was a polystyrene based thermoset SMP resin system with a T_g of 62 °C commercially sold by CRG Industries under the name of *Veriflex*. A hardening agent distributed by the same company was then added to the SMP resin. The mixture was blended for 10 min before it was poured into a $229 \times 229 \times 12$ mm^3 steel mold and placed into a vacuum chamber at 40 kPa for 20 min for removal of any air pockets introduced during the mixing process. The resin was then cured in an oven at 79 °C for 24 h, followed by 6 h at 107 °C. After curing, the SMP panel was de-molded and cut into $30 \times 30 \times 12$ mm^3 block specimens for further testing.

2.2. Dynamic mechanical analysis

In order to determine the glass transition zone of the SMP, the dynamic mechanical analysis (DMA) test was conducted on a DMA 2980 tester from TA instruments per ASTM D 4092. A rectangular sheet with dimensions of $17.5 \times 11.9 \times 1.20$ mm^3 was placed into a DMA single cantilever clamping fixture. A small dynamic load at 1 Hz was applied to a platen and the temperature was ramped from room temperature to 120 °C at a rate of 3 °C/min. The amplitude was set to be 15 μm.

2.3. Coefficient of thermal expansion measurement

The linear thermal expansion coefficient was measured by using a linear variable differential transducer (LVDT, Cooper Instruments LDT 200 series) system to record the specimen surface displacement and a Yokagawa DC100 data acquisition system to collect the thermal couple measurement of the temperature change. The temperature was ramped from room temperature to 100 °C at an average heating rate of 0.56 °C/min. After equilibrated for 30 min, the sample was naturally cooled down to room temperature.

2.4. Programming by isothermal flat-wise uniaxial compression test

As discussed previously, we proposed to program the specimens at a temperature well below the T_g of the SMP, instead of the typical lengthy programming process above T_g. In this study, room temperature (20 °C) was adopted for programming. The programming was conducted by a uniaxial compression test. Uniaxial flat-wise compression was performed with a MTS QTEST150 electromechanical frame outfitted with a moveable furnace (ATS heating chamber) per the ASTM C 365 standard at a displacement rate of 1.3 mm/min to the test prestrain level. Temperature control and monitor were achieved through a thermocouple placed in the chamber near the SMP specimen. Stress–strain responses were then generated for different prestrain levels and stress relaxation time. In this study, three prestrain levels (5%, 10%, and 30%), corresponding to the elastic zone (5%) and post-yielding zone (10% and 30%), respectively, were selected. The stress relaxation time was determined to be 0, 30, 120, and 260 min for the 5% prestrain level, and 0, 5, 15, 30, and 120 min for the 10% and 30% prestrain levels. At least three effective specimens were tested for each prestrain level and stress relaxation time.

2.5. Free shape recovery test

Once the specimens were programmed, unconstrained strain recovery test was then implemented, where the compressed SMP specimen was heated to $T_{high}=79$ °C at an average heating rate of $q=0.82$ °C/min. The same LVDT system was used to track the movement of the specimen during heating.

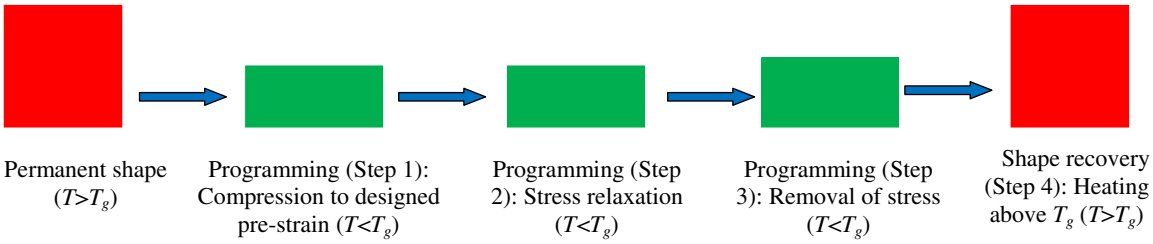

Fig. 1. A schematic of the four-step thermomechanical cycle (programming (Steps 1–3) and shape recovery (Step 4)).

The thermomechanical cycle including programming and shape recovery was schematically shown in Fig. 1. It is seen that the programming consists of three steps at a fixed glassy temperature (room temperature in this study): compression to the designed prestrain (Step 1), stress relaxation (Step 2), and removal of loading (Step 3). Obviously, depending on the relaxation time, the entire programming takes from minutes to a couple of hours, instead of the typical way of programming, which requires a refined temperature control and over 10 h of programming time (Li and Nettles, 2010; Li and Uppu, 2010). For Step 4, shape recovery, it is the same as the typical approach.

2.6. Environmental conditioning tests

The capability for the SMP to maintain its shape fixity has been well established for specimens programmed by the typical programming approach. However, it is not clear about the functional stability of the SMP programmed at a temperature below T_g. In other words, it is not clear if the nonequilibrium configuration created by cold-compression programming can be maintained or not under various environmental attacks. The stability of the temporary shape of the SMP specimens was investigated, respectively, under specific conditions of water immersion, ultraviolet light (UV) exposure and a combination of these two conditions. For the water immersion test, one programmed specimen was immersed in a cup of drinking water. The water level was about 2.5 cm above the surface of the specimen. For the UV exposure test, one programmed specimen was put in the same plastic cup without water. A 300-W Mog Base UV lamp, which had a wavelength ranging from 280 to 340 nm (mixed UV-A and UV-B light), was placed about 30 cm away from the transparent plastic cup. For the combined water immersion and UV exposure test, again one programmed specimen was immersed in the same transparent plastic cup containing the same amount of drinking water. At the same time, the specimen was exposed to the same UV source with the same intensity. The specimens were monitored regularly during a period of up to 3 months in order to record any dimension changes. In the first two weeks, the dimension of the specimens was measured everyday and after that, the dimension was recorded every week. After 3 months of environmental attacks, the specimens were recovered using the same procedure as the non-attacked specimens.

3. Experimental results

3.1. DMA test results

The experimental results in Fig. 2 illustrate the storage modulus and loss modulus of the SMP as functions of temperature. The glass transition zone and T_g can be found from the storage modulus per ASTM D 4092. The intersection between the tangent at the inflection point and the extrapolated tangent at the glassy state defines the lower limit and the intersection between the tangent at the inflection point and the extrapolated tangent at the rubbery plateau defines the upper limit of the glass transition zone. The average value in between them defines the glass transition temperature T_g=67.78 °C. The listed value of T_g=62 °C by the distributor was determined by differential scanning calorimetry (DSC), which was about 4 °C lower than their DMA results. Therefore, the T_g provided by the manufacturer is consistent with our test results.

3.2. Uniaxial strain-controlled compression programming

The strain evolution during the material programming process, including the first three steps of the entire thermomechanical cycle in Fig. 1, is presented in Fig. 3. Obviously, the shape fixity highly depends on the prestrain levels. SMP specimens programmed by 5% prestrain level cannot fix a temporary shape regardless of the length of the stress relaxation time. Upon removal of the load, immediate full spring-back is observed. For specimens programmed by 30% prestrain, however, a decent amount of strain is preserved, even when the load is instantly removed (zero relaxation time). With zero stress relaxation time, the shape fixity is still about 73%. Therefore, the prestrain level plays a key role in programming at glassy temperature. As documented in a previous study (Li and Nettles, 2010), the uniaxial compression yielding strain of the same thermosetting SMP is about 7% at the same glassy temperature. Obviously, 5% prestrain falls in

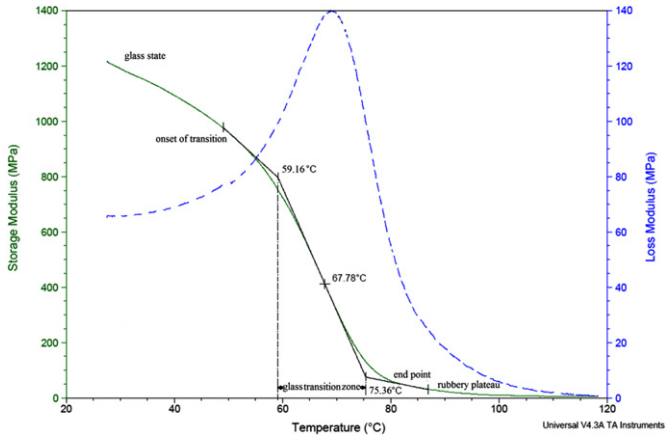

Fig. 2. DMA results as functions of temperature: (a) solid green line-storage modulus and (b) dash blue line-loss modulus. (For interpretation of the references to color in this figure legend, the reader is referred to the web version of this article.)

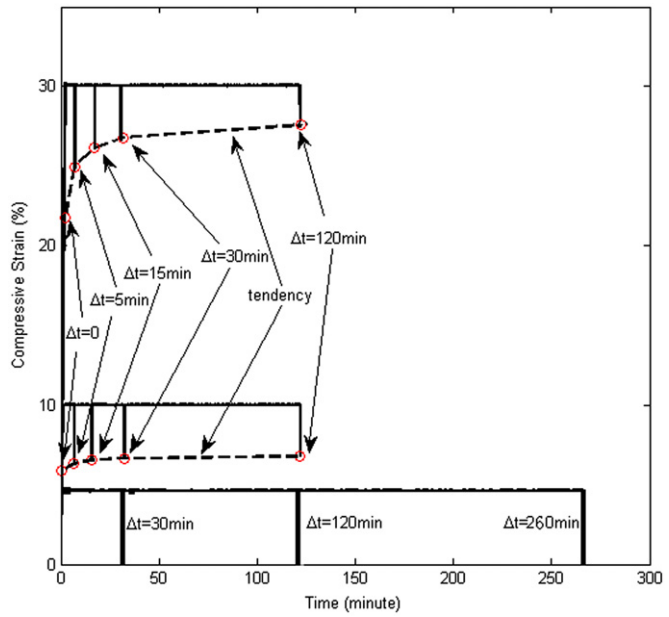

Fig. 3. Shape fixity results at temperature below T_g for specimens programmed at different prestrain levels (5%, 10%, and 30%).

the elastic region of the SMP. Therefore, immediate full spring-back occurs regardless of the relaxation time held. At 30% prestrain, the SMP specimen already yields and thus is able to maintain a decent temporary fixed strain even without stress relaxation. Therefore, a post-yielding prestrain level determines the success of the programming at glassy temperature.

It can also be observed from Fig. 3 that, with 30% prestrain, a longer stress relaxation time in Step 2 tends to enhance the shape fixity ratio. As the relaxation time continuously increases, the shape fixity asymptotically approaches an upper bound, which is equal to the difference between the prestrain and elastic spring-back (ratio of the relaxed stress over the relaxed modulus). Further increase in the relaxation time can hardly bring up any significant increase in the shape fixity ratio.

With 10% prestrain, which is about 3% higher than the yield strain, a tendency similar to 30% prestrain is observed. Therefore, as long as the prestrain is over the yield strain, a certain amount of shape fixity can be realized. Of course, as the prestrain increases, the shape fixity also increases. For example, at zero stress relaxation time, the shape fixity is about 62.5% for 10% prestrain level, which is lower than the corresponding shape fixity of 73% for 30% prestrain level. It is also observed that the shape fixity with 10% prestrain plateaus earlier than that with 30% prestrain as stress relaxation time increases, possibly due to less viscoelastic and viscoplastic deformation with lower prestrain level.

3.3. Environmental conditioning test

The environmental attack test detected no change in specimen dimensions for any environmental conditions during the tests. Free shape recovery test showed almost the same recovery ratio as those non-attacked specimens. Since the observation time was up to 3 months and the environment conditions covered the most common working conditions, the stability of the nonequilibrium configuration created by cold-compression programming should be well confirmed. In other words, the temporary shape of the thermosetting SMP programmed at temperature below T_g is stable.

3.4. Free recovery test

Fig. 4 shows the entire thermomechanical cycles, including the unconstrained strain recovery during the heating process (Step 4 in Fig. 1). From Fig. 4 (a), which is programmed by 30% prestrain, it is observed that initially the programmed specimen only shows a slight and gradual thermal expansion, while as the temperature approaches T_g, the influence of the entropy change is becoming dominant, leading to a rapid strain recovery. At temperatures well above T_g, most of the prestrain has been released and the strain converges to a stabilized value. It is interesting to note that a similar

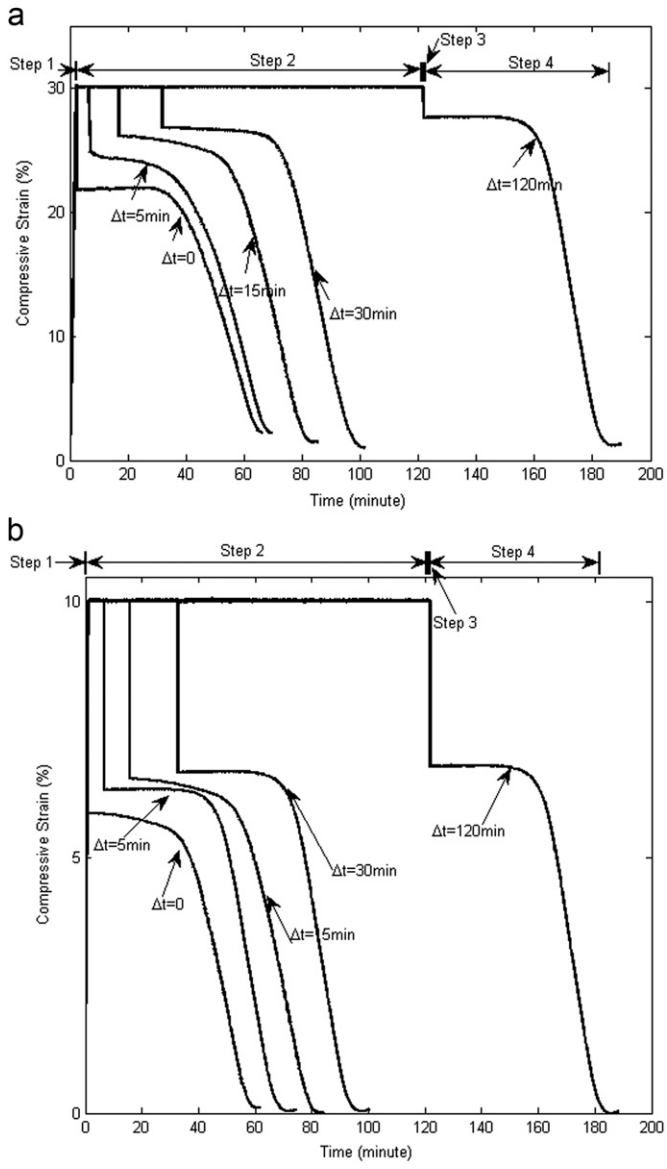

Fig. 4. Strain–time response during the entire thermomechanical cycle for specimens programmed with (a) 30% and (b) 10% prestrain (the four steps for the specimen with 120 min of stress relaxation time during programming are also shown).

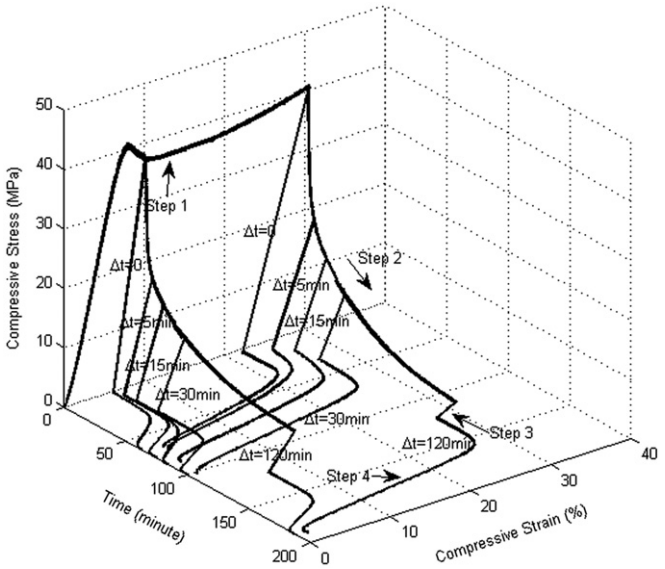

Fig. 5. 3-D thermomechanical cycle in terms of stress–strain–time for different stress relaxation time with prestrain levels of 10% and 30%.

sigmoidal-type strain recovery path is shared by all the specimens with different relaxation time during programming, implying that the strain release mechanism is generally independent of the holding time during programming. With 10% prestrain (Fig. 4(b)), the shape recovery follows a tendency similar to that with 30% prestrain. A noticeable difference exists in the shape recovery ratio. With the 10% prestrain, the shape recovery ratio is about 100%, regardless of the stress relaxation time during programming; with the 30% prestrain, there is a small amount of strain that cannot be recovered. A possible reason is that, with the 30% prestrain, some damage may have been created within the SMP specimen, which cannot be recovered during free shape recovery. Overall, the shape memory capability of the thermosetting SMP programmed by clod-compression is considerable. In other words, the approach of programming at glassy temperature is much simpler and easier with a considerable shape memory capability, and thus should be applied in practice.

The 3-D stress–strain–time behaviors for the entire themomechanical cycle, which include the three-step cold-compression programming process and the one step heating recovery, are shown in Fig. 5, for both the 10% and 30% prestrain levels. An extremely nonlinear, time and temperature dependent constitutive behavior is revealed. In-depth understanding of this complex thermomechanical behavior demands comprehensive constitutive modeling, which is developed in the following section.

4. Constitutive modeling

4.1. General consideration

As previously documented the molecular resistance to inelastic deformation for SMPs below the glass transition temperature (T_g) mainly originates from two sources: the intermolecular resistance to segmental rotation and the entropic resistance to molecular alignment (Boyce et al., 1989, 2001). The four-step thermomechanical cycle shown in Fig. 5 can be analyzed as follows. It is assumed that the plastic flow does not commence until the stressed material completely overcomes the free energy barrier to the molecular chain mobility, a restriction imposed on molecular chain motion from neighboring chains. Following the initial yield, molecular alignment occurs and subsequently alters the configurational entropy of the material (Step 1). Since the plastic straining develops in a rate-dependent manner, the length of relaxation time physically indicates the degree of the nonequilibrium configuration (Step 2). A relaxed configuration is then obtained after elastically unloading to a stress free state (Step 3). Due to the high material viscosity and vanishing chain mobility at the glassy programming temperature, the nonequilibrium structure is prevented from relaxing to the equilibrium state in an observable time frame, resulting in a retained temporary shape at the end of Step 3. Upon heating to above T_g the viscosity decreases and chain mobility increases. The thermodynamically favorable tendency of increasing entropy allows the material to restore its equilibrium configuration and thus achieve shape recovery (Step 4).

Based on this understanding, a mechanism-based constitutive model by incorporating the nonlinear structural relaxation model into the continuum finite-deformation thermoviscoelastic theory was developed as follows. The aim of this effort was to establish a quantitative understanding of the shape memory behavior of the thermally responsive

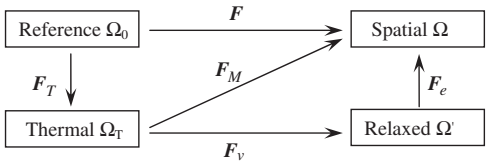

Fig. 6. An analogous decomposition scheme for the deformation gradient.

thermoset SMP programmed at temperatures below T_g. Therefore, to keep matters simple, several basic assumptions were made in this study:

(1) The SMP system is considered to be macroscopically isotropic and homogeneous. A uniform stress field assumption is held.
(2) Heat transfer in the material is not considered. The temperature is then treated as uniform over the entire body.
(3) The structural relaxation and inelastic behavior of the material are assumed to be solely dependent on the temperature, time and stress.
(4) The material is assumed to be without any damage during the thermomechanical cycle.

4.2. Deformation response

As illustrated in Fig. 6, any arbitrary thermomechanical path can be considered as a transition of the material between an initial reference configuration of an undeformed and unheated continuum body denoted by $\boldsymbol{\Omega}_0$ and a spatial configuration $\boldsymbol{\Omega}$ of the deformed body which may have also experienced a certain temperature change. It is assumed that the configuration $\boldsymbol{\Omega}_0$ is either in thermodynamic equilibrium in rubbery state or in a stress-free glassy configuration originated from mechanically unconstrained cooling from high temperature. A deformation gradient $\boldsymbol{F}=\partial x/\partial \boldsymbol{X}$ represents the tangent of a general nonlinear mapping $\boldsymbol{x}=\boldsymbol{x}(\boldsymbol{X}(t),T(t),t)$ of a material point from $\boldsymbol{\Omega}_0$ to $\boldsymbol{\Omega}$. This deformation mapping is then considered to be a combination of a thermal deformation and a mechanical deformation, which can be separated through a multiplicative decomposition scheme (Lu and Pister, 1975; Lion, 1997):

$$\boldsymbol{F}=\boldsymbol{F}_M\boldsymbol{F}_T \tag{1}$$

Here $\boldsymbol{F}_M$ defines the mechanical deformation gradient; $\boldsymbol{F}_T$ defines the mapping path from $\boldsymbol{\Omega}_0$ to $\boldsymbol{\Omega}_T$, an intermediate heated configuration. Because the material is assumed to be isotropic, the thermal deformation gradient can be expressed as

$$\boldsymbol{F}_T=J_T^{1/3}\boldsymbol{I} \tag{2}$$

where $J_T=\det(\boldsymbol{F}_T)$ is the determinant of the thermal deformation gradient, representing the volumetric thermal deformation.

To separate the elastic and viscous response, we further introduce the multiplicative split of the mechanical deformation gradient into elastic and viscous components (Sidoroff, 1974; Lion, 1997):

$$\boldsymbol{F}_M=\boldsymbol{F}_e\boldsymbol{F}_v \tag{3}$$

Although a discrete spectrum of nonequilibrium processes $\boldsymbol{F}_M^i=\boldsymbol{F}_e^i\boldsymbol{F}_v^i$ $(i=1,\ldots,N)$ (Govindjee and Reese, 1997) would be more appropriate to describe the general behavior of the real solid materials, only single stress relaxation is considered in the following derivation for the sake of convenience. The viscous part of the velocity gradient is then defined as

$$\boldsymbol{L}_v=\dot{\boldsymbol{F}}_v\boldsymbol{F}_v^{-1}=\boldsymbol{D}_v+\boldsymbol{W}_v \tag{4}$$

where $\boldsymbol{D}_v$ is the symmetric part of $\boldsymbol{L}_v$, representing the plastic stretch of the velocity gradient and $\boldsymbol{W}_v$ is the asymmetric component, representing the plastic spin. By applying the polar decomposition, we can also split $\boldsymbol{F}_e$ into a stretch ($\boldsymbol{V}_e$) and a rotation ($\boldsymbol{R}_e$) as

$$\boldsymbol{F}_e=\boldsymbol{V}_e\boldsymbol{R}_e \tag{5}$$

4.3. Structural relaxation response

A fictive temperature T_f based approach firstly introduced by Tool (1946) has been proved to be extremely successful in supplying the information about the free volume or the structure in the formulation of the free energy density. The fictive temperature T_f is an internal variable to characterize the actual thermodynamic state during the glass transition, defined as the temperature at which the temporary nonequilibrium structure at T is in equilibrium (Nguyen et al., 2008). It was

assumed that the rate change of the fictive temperature is proportional to its deviation from the actual temperature and the proportionality factor depends on both T and T_f (Narayanaswamy, 1971), as indicated in the evolution equation (Tool, 1946):

$$\frac{dT_f}{dt} = K(T,T_f)(T-T_f) \tag{6}$$

The Narayanaswamy–Moynihan model (NMM), discussed in details by Donth and Hempel (2002), is an improvement for this approach. Instead of postulating a simple exponential relaxation mechanism governed by a single relaxation time (Tool, 1946), the non-exponential structural relaxation behavior as well as the spectrum effect were studied. It is assumed that the whole thermal history $T(t)$ starts from a thermodynamic equilibrium state where $T(t_0)=T_f(t_0)$. And Tool's fictive temperature is defined by

$$T_f(t) = T(t) - \int_{t_0}^{t} \varphi(\Delta\varsigma)\, dT(t) \tag{7}$$

The response function is chosen, according to Moynihan et al. (1976), in a manner of a Kohlrausch function (Kohlrausch, 1847), and the value of β describes the non-exponential characteristic of the relaxation process:

$$\varphi = \exp\left[-(\Delta\varsigma)^{\beta}\right], \quad 0<\beta\le 1 \tag{8}$$

The dimensionless material time difference $\Delta\varsigma$ is introduced to linearize the relaxation process:

$$\Delta\varsigma = \varsigma(t) - \varsigma(t') = \int_{t'}^{t} \frac{dt}{\tau_s} \tag{9}$$

where the structural relaxation time τ_s, a macroscopic measurement of the molecular mobility of the polymer, accounts for the characteristic retardation time of the volume creep (Hempel et al., 1999; Nguyen et al., 2008). As presented earlier that the structural relaxation in terms of τ_s is controlled by both the actual temperature T and the fictive temperature T_f, a Narayanaswamy mixing parameter x was introduced to weigh their individual influence (Narayanaswamy, 1971):

$$\tau_s = \tau_0 \exp\left[B(T_g - T_\infty)^2 \left(\frac{x}{T-T_\infty} + \frac{1-x}{T_f-T_\infty}\right)\right], \quad 0<x\le 1 \tag{10}$$

It can be observed that the term of $(1-x)$ describes the contribution of T_f. Here, T_g is the glass transition temperature. T_∞ denotes the Vogel temperature, defined as (T_g-50) (°C). τ_0 corresponds to the reference relaxation time at T_g. And B is the local slope at T_g of the trace of time–temperature superposition shift factor in the global William–Landel–Ferry (WLF) equation (William et al., 1955).

After obtaining the evolution profile of T_f, we can then evaluate the isobaric volumetric thermal deformation corresponding to a temperature change from T_0 to T (Narayanaswamy, 1971; Scherer, 1990; Nguyen et al., 2008):

$$J_T(T,T_f) = 1 + \alpha_r(T_f - T_0) + \alpha_g(T - T_f) \tag{11}$$

where α_r and α_g represent the long-time volumetric thermal expansion coefficients of the material in the rubbery state and the short-time response in the glassy state, respectively.

4.4. Stress response

The mechanical behavior of amorphous glassy polymers under various temperature conditions has been extensively studied by numerous researchers (Boyce et al., 1988a, b, 1989, 2001; Treloar, 1958; Govindjee and Simo, 1991; Arruda and Boyce, 1993; Bergstrom and Boyce, 1998; Miehe and Keck, 2000; Qi and Boyce, 2005). Although other approaches can still accommodate the present constitutive framework, the method by Boyce and co-workers is adopted in this study to model the general stress–strain behavior of the SMPs.

As demonstrated previously, the overall mechanical resistance to the straining of a polymer mainly comes from two distinct sources: the temperature rate dependent intermolecular resistance and the entropy driven molecular network orientation resistance. It is therefore possible to capture this nonlinear behavior by decomposing the stress response into an equilibrium time-dependent component $\boldsymbol{\sigma}_{ve}$ representing the viscoplastic behavior and an equilibrium time-independent component $\boldsymbol{\sigma}_n$ representing the rubber-like behavior. The two stress components can be represented by a three-element conceptual model schematically illustrated in Fig. 7 for a one-dimensional analog. An elastic–viscoplastic component consists of an Eyring dashpot monitoring an isotropic resistance to chain segment rotation and a linear spring used to characterize the initial elastic response, while a paralleled nonlinear hyperelastic element accounts for the orientation strain hardening behavior.

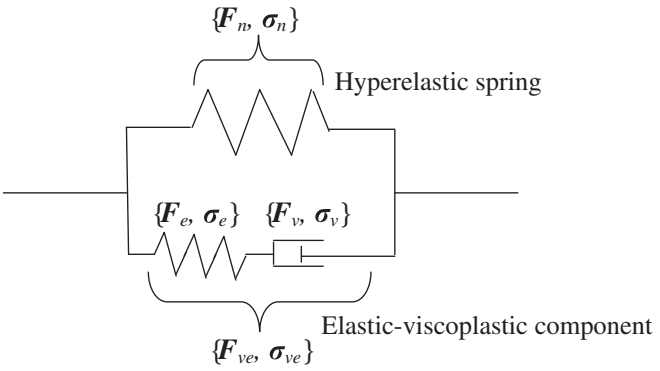

Fig. 7. A linear rheological analog illustration for stress response.

If we further denote the deformation gradient acting on the elastic–viscoplastic component by $\boldsymbol{F}_{ve}$ and the deformation gradient acting on the network orientation spring by $\boldsymbol{F}_n$, the following constitutive relations are revealed:

$$\boldsymbol{\sigma} = \boldsymbol{\sigma}_{ve} + \boldsymbol{\sigma}_n \tag{12}$$

$$\boldsymbol{\sigma}_{\mathrm{ve}} = \boldsymbol{\sigma}_e = \boldsymbol{\sigma}_v \tag{13}$$

$$\boldsymbol{F}_{ve} = \boldsymbol{F}_n = \boldsymbol{F}_M \tag{14}$$

$$\boldsymbol{F}_{ve} = \boldsymbol{F}_e \boldsymbol{F}_v \tag{15}$$

Then the equilibrium response acting on the network orientation element can be defined following the Arruda–Boyce eight chain model (Arruda and Boyce, 1993) as:

$$\boldsymbol{\sigma}_n = \frac{1}{J_n}\mu_r \frac{\lambda_L}{\lambda_{chain}} \mathcal{L}^{-1}\left(\frac{\lambda_{chain}}{\lambda_L}\right)\overline{\boldsymbol{B}}' + k_b(J-1)\boldsymbol{I} \tag{16}$$

where μ_r is the initial hardening modulus, and k_b denotes the bulk modulus to account for the incompressibility of rubbery behavior. Because most amorphous polymers exhibit vastly different volumetric and deviatoric behavior, the volumetric and deviatoric contributions are considered separately by taking out the volumetric strain through the split formulation (Flory, 1961; Simo et al., 1985):

$$\overline{\boldsymbol{F}}_n = J_n^{-1/3}\boldsymbol{F}_n \tag{17}$$

where $J_n = \det(\boldsymbol{F}_n)$. $\overline{\boldsymbol{B}} = \overline{\boldsymbol{F}}_n \overline{\boldsymbol{F}}_n^T$ is the isochoric left Cauchy–Green tensor, and $\overline{\boldsymbol{B}}' = \overline{\boldsymbol{B}} - \frac{1}{3}\bar{I}_{n1}\boldsymbol{I}$ represents the deviatoric component of $\overline{\boldsymbol{B}}$. $\bar{I}_{n1} = tr(\overline{\boldsymbol{B}})$ is the first invariant of $\overline{\boldsymbol{B}}$. $\lambda_{chain} = \sqrt{\bar{I}_{n1}/3}$ is the effective stretch on each chain in the eight-chain network. λ_L is the locking stretch representing the rigidity between entanglements. The Langevin function $\mathscr{L}$ is defined by:

$$\mathcal{L}(\beta) = \coth(\beta) - \frac{1}{\beta} \tag{18}$$

whose inverse leads to the feature that the stress increases dramatically as the chain stretch approaches its limiting extensibility λ_L.

The nonequilibrium stress response acting on the elastic–viscoplastic component can be determined through the elastic contribution $\boldsymbol{F}_e$:

$$\boldsymbol{\sigma}_{ve} = \boldsymbol{\sigma}_e = \frac{1}{J_e} L^e(\ln \boldsymbol{V}_e) \tag{19}$$

where $J_e = \det(F_e)$, and $\boldsymbol{L}^e = 2G\mathcal{J} + \lambda \boldsymbol{I} \otimes \boldsymbol{I}$ is the fourth order isotropic elasticity tensor. G and λ are Lamé constants, $\mathcal{J}$ is the fourth order identity tensor and $\boldsymbol{I}$ is the second order identity tensor.

4.5. The viscous flow

As proposed earlier, the molecular process of a viscous flow is to overcome the shear resistance of the material for local rearrangement. Therefore, a plastic shear strain rate $\dot{\gamma}_v$ is given to help constitutively prescribe the viscous stretch rate $\boldsymbol{D}_v$ as:

$$\boldsymbol{D}_v = \dot{\gamma}_v \boldsymbol{n} \tag{20}$$

where

$$\boldsymbol{n}=\frac{\boldsymbol{\sigma}'_{ve}}{\sqrt{\boldsymbol{\sigma}'_{ve}:\boldsymbol{\sigma}'_{ve}}}=\frac{\boldsymbol{\sigma}'_{ve}}{\|\boldsymbol{\sigma}'_{ve}\|}$$

is the normalized deviatoric portion of the nonequilibrium stress. It states that the viscous stretch rate scales with the plastic shear strain rate and evolves in the direction of the flow stress.

Taking into account that the non-Newtonian fluid relationship must be valid for the dashpot of the mechanical model, the shear strain rate $\dot{\gamma}_v$ can be formulated in an Eyring model (Eyring, 1936) with the temperature dependence in a WLF kinetics manner:

$$\dot{\gamma}_v=\frac{s}{\eta_g}\frac{T}{Q}\exp\left(\frac{c_1(T-T_g)}{c_2+T-T_g}\right)\sinh\left(\frac{Q}{T}\frac{\overline{\tau}}{s}\right) \tag{21}$$

here $\overline{\tau}=\|\boldsymbol{\sigma}'_{ve}\|/\sqrt{2}$ is defined as the equivalent shear stress; c_1, c_2 are the two WLF constants; Q is the activation parameter; s represents the athermal shear strength; and η_g denotes the reference shear viscosity at T_g. The evolution Eq. (21) reveals the nature of the viscoplastic flow to be temperature-dependent and stress activated.

More recently, Nguyen et al. (2008) further extended the viscous flow rule to a structure dependent glass transition region by introducing the fictive temperature T_f into the temperature dependence:

$$\dot{\gamma}_v=\frac{s}{\eta_g}\frac{T}{Q}\exp\left(c_1\left(\frac{c_2(T-T_f)+T(T_f-T_g)}{T(c_2+T-T_{g)}}\right)\right)\sinh\left(\frac{Q}{T}\frac{\overline{\tau}}{s}\right) \tag{22}$$

It can be observed that once the material reaches equilibrium where $T_f=T$, Eq. (22) will reduce to Eq. (21) for a structure independent time–temperature shift factor.

As extensively documented, upon yielding the initial rearrangement of the chain segments alters the local structure configuration, resulting in a decrease in the shear resistance. To further feature the macroscopic post-yield strain softening behavior, the phenomenological evolution rule for the athermal shear strength s proposed by Boyce et al. (1989) is implemented,

$$\dot{s}=h\left(1-\frac{s}{s_s}\right)\dot{\gamma}_v \tag{23}$$

The initial condition $s=s_0$ applies. Here s_0 denotes the initial shear strength, while s_s denotes the saturation value. h is the slope of the yield drop with respect to plastic strain. It should be noted that a softening characteristic can only be captured when $s_0>s_s$ holds.

4.6. General remarks

For completeness, the constitutive relations for the sophisticated temperature and time dependent thermomechanical behavior of the thermally activated thermoset SMP are summarized in Table 1. The comprehensive model considers the material mechanical response in a manner of structure dependent thermoviscoelasticity and is capable of capturing the important features of the polymer behavior such as yielding, strain softening and strain hardening. However, it should be noted that since our aim is just to establish a thermomechanic framework for the extraordinary characteristics of SMPs programmed at glassy temperature, the present constitutive model is comparatively simple to the real SMP behavior. Several factors such as heat conduction and pressure on the structure relaxation response are not taken into account.

Table 1
Summary of the thermoviscoelastic–viscoplastic model.

Deformation response	$\boldsymbol{F}=\boldsymbol{F}_e\boldsymbol{F}_v\boldsymbol{F}_T$ $\boldsymbol{F}_T=J_T^{-1/3}\boldsymbol{I}$
Structure relaxation	$T_f(t)=T(t)-\int_{t_0}^{t}\varphi(\Delta\varsigma)dT(t)$ $\varphi=\exp\left[-(\Delta\varsigma)^{\beta}\right]$ $\Delta\varsigma=\varsigma(t)-\varsigma(t')=\int_{t'}^{t}\frac{dt}{\tau_s}$ $\tau_s=\tau_0\exp\left[B(T_g-T_\infty)^2\left(\frac{x}{T-T_\infty}+\frac{1-x}{T_f-T_\infty}\right)\right]$
Stress response	$\boldsymbol{\sigma}=\boldsymbol{\sigma}_{ve}+\boldsymbol{\sigma}_n$ $\boldsymbol{\sigma}_n=\frac{1}{J_n}\mu_r\frac{\lambda_L}{\lambda_{chain}}\mathcal{L}^{-1}\left(\frac{\lambda_{chain}}{\lambda_L}\right)\overline{\boldsymbol{B}}'+k_b(J-1)\boldsymbol{I}$ $\boldsymbol{\sigma}_{ve}=\frac{1}{J_e}L^e(\ln\boldsymbol{V}_e)$
Viscous flow rule	$\boldsymbol{D}_v=\dot{\gamma}_v\boldsymbol{n}$ $\dot{\gamma}_v=\frac{s}{\eta_g}\frac{T}{Q}\exp\left(c_1\left(\frac{c_2(T-T_f)+T(T_f-T_g)}{T(c_2+T-T_{g)}}\right)\right)\sinh\left(\frac{Q}{T}\frac{\overline{\tau}}{s}\right)$

A single nonequilibrium stress relaxation process is also assumed for the sake of convenience, yet multiple relaxation mechanism (i.e., more separate Maxwell elements in Fig. 7) are required to distinguish the long-range entropic stiffening process and the short-range viscoplastic flow induced strain-hardening behavior.

5. Results and discussions

5.1. Model validation

The constitutive relations were then coded and implemented into the MATLAB program of which the flowchart is illustrated in Appendix A to simulate the corresponding experimental data reported earlier. The model parameters were obtained through various mechanical testings. Detailed parameter identification procedures are briefly described in Appendix B. The final values of these parameters are listed in Table 2. The mathematical formulation for 1-D compression is demonstrated in Appendix C.

Based on the parameters identified in Table 2, the numerical simulation result, which covers the entire thermo-mechanical profile of the SMP programmed at 30% prestrain and is for different relaxation histories in a strain–time scope, is shown in Fig. 8(a). The material was initially stressed to the pre-defined strain level after overcoming the yielding point and experiencing a slight strain-softening followed by a significant strain hardening (Step 1) phenomenon. After that it was held with different time periods of relaxation for plastic strain development (Step 2). Finally the remaining stress was instantly removed, leading to a stress-free state (Step 3). Lengthy relaxation seemly enhanced the level of the strain fixity. The stored deformation was then released and the original shape recovered during a subsequent heating process (Step 4).

From Fig. 8(a), the model simulation generally has a reasonable agreement with the test results. It proves that the model is capable of capturing the basic nonlinear material behavior of the SMP during such a thermomechanical cycle, although it can be observed that the real SMP samples failed to achieve the full recovery as indicated by the prediction. The reason for this discrepancy may come from a couple of sources. Considering the large peak compressive stress applied during programming (about 40 MPa in Fig. 5 and Fig. 8(a)), some irreversible damage may have been induced in the SMP specimen. Also the deficiency of the single relaxation assumption appears evident in the discrepancies between the simulation and experiments when the relaxation time is insufficient. This can be validated by Fig. 8(a) that when the relaxation time is short, the discrepancy is large; when the relaxation time is long enough (120 min), the discrepancy becomes comparatively small. Therefore, a spectrum of multiple nonequilibrium processes would be required to describe the actual stress relaxation process of a real thermosetting SMP.

In this study, the same parameters calibrated in modeling the constitutive behavior of the SMP programmed by 30% prestrain level were also used to predict the thermomechanical behavior of the same SMP programmed by 10% prestrain level; see Fig. 8(b). It is clear that, with the same set of parameters, the model well predicted the constitutive behavior of the SMP programmed by 10% prestrain. This further validated the developed model.

Table 2
Material parameters of the preliminary constitutive model.

Model parameters	Values
T_g (°C) glass transition temperature	62
T_0 (°C) programming temperature	20
Δt (minute) relaxation time	0/5/15/30/120
α_g ($10^{-4}\circ C^{-1}$) volumetric CTE of glassy state	5.462
α_r ($10^{-4}\circ C^{-1}$) volumetric CTE of rubbery state	8.441
G (MPa) glassy shear modulus	196.4
λ (MPa) Lamé constant for glassy state	785.7
μ_r (MPa) rubbery modulus	1.2
k_b (MPa) bulk modulus	1000
λ_L locking stretch	0.95
μ_g (MPa s^{-1}) reference shear viscosity at T_g	1550
s_0 (MPa) initial shear strength.	35
s_s (MPa) steady-state shear strength	33
Q/s_0 (K/MPa) flow activation ratio	380
h (MPa) flow softening constant	250
c_1 first WLF constant	25.8
c_2 (°C) second WLF constant	90
τ (s) structure relaxation characteristic time	200
x NMM constant	0.95
β Kohlrausch index	0.95

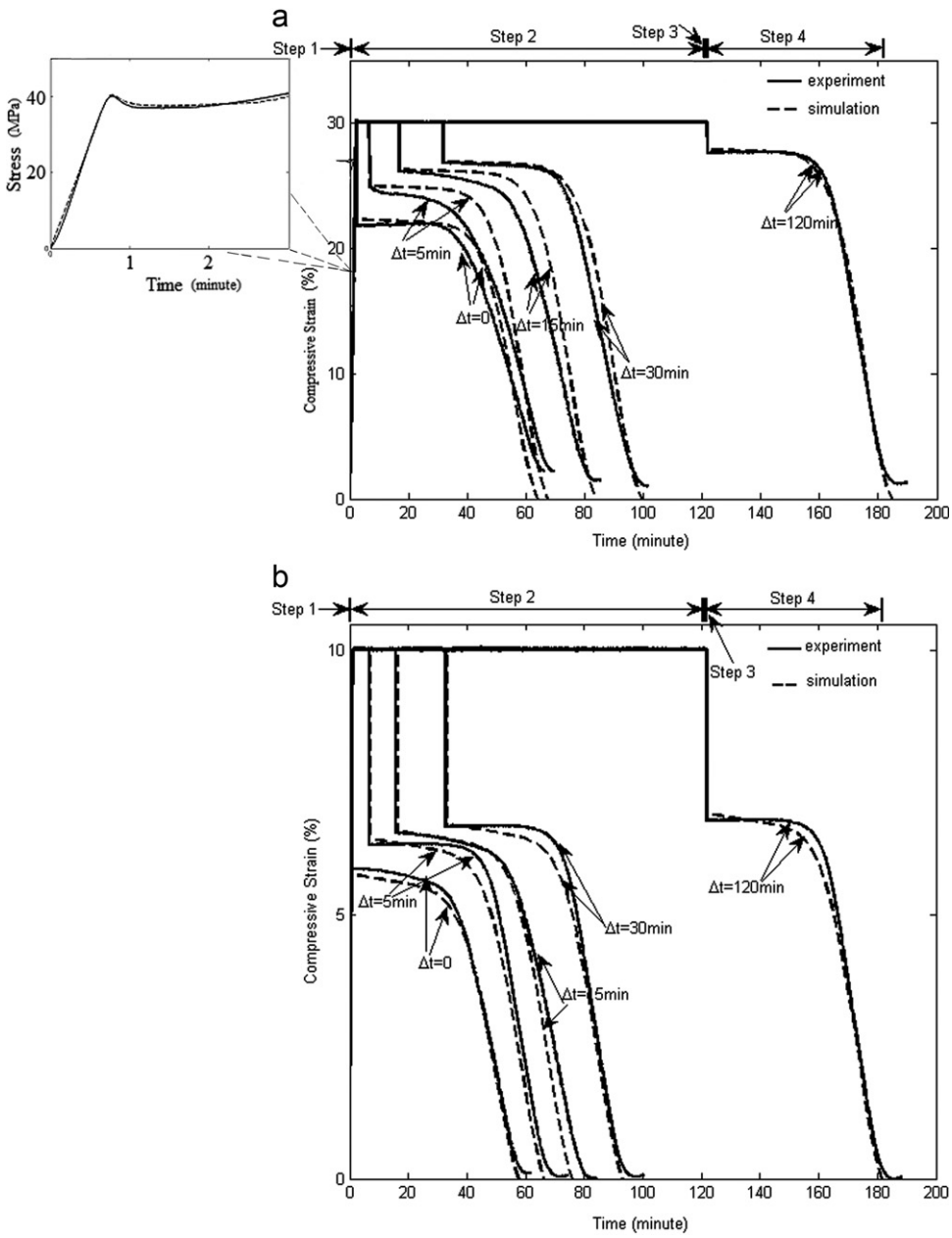

Fig. 8. Numerical simulation for samples with (a) 30% prestrain and (b) 10% prestrain during the entire thermomechanical cycle (the four steps for the entire thermomechanical cycle for the specimen with 120 min of stress relaxation time during programming are also shown).

5.2. Prediction and discussion

To demonstrate that the shape memory response of the SMP has a strong dependence on the structural evolution, the influence of the temperature profile has been investigated through the unconstrained recovery simulations.

5.2.1. Dependence on the heating rate

Fig. 9 exhibits the free recovery prediction results for two different heating rates $q=0.6$ and 3 °C/min. It is observed that a faster heating rate shifts the initiation of the recovery process to a higher temperature and leads to a more gradual temperature dependence at the start of the strain release, but hardly affects the final recovery ratio.

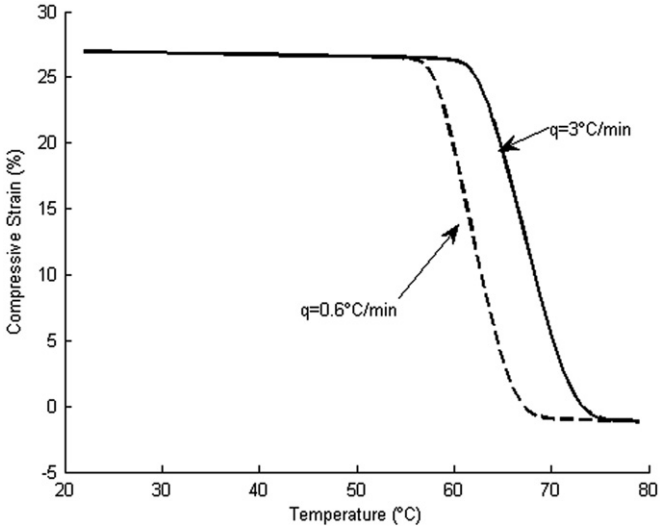

Fig. 9. Recovery strain as a function of temperature for different heating rates.

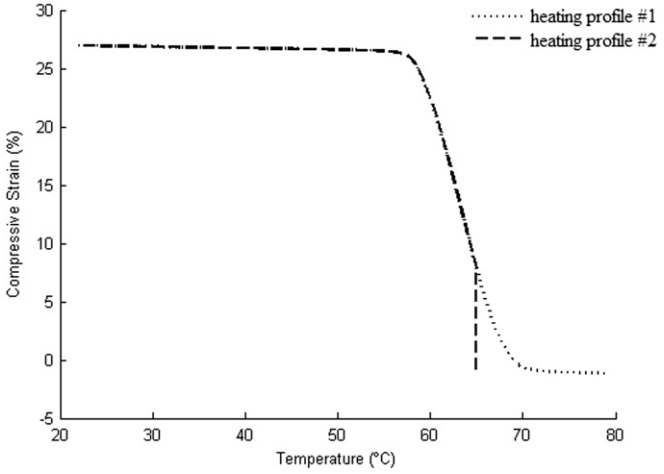

Fig. 10. Recovery strain as a function of temperature for different heating profiles.

5.2.2. Dependence on the heating history

Besides the heating rate, the heating profile also influences the structure evolution. The calculation results for two types of heating profiles are shown in Fig. 10. Heating profile #1 represents a heating profile from 22 to 79 °C with a constant heating rate of $q=1$ °C/min; while heating profile #2 represents a heating profile from 22 to 68 °C with a constant heating rate of $q=1$ °C/min and followed with a 50 min soaking period. It exhibits that although heating profile #2 does not reach the same high temperature of 79 °C as that of the heating profile #1, it still reaches the same recovery strain level after the adequate soaking. This is an indication of time–temperature equivalence.

5.2.3. Dependence on the programming temperature T_0

The effect of the programming temperature T_0 is shown in Fig. 11. The SMP samples are considered to be programmed at 20 and 40 °C, respectively for the same relaxation time period of 20 min. Two cases are considered. For Case (a), shape recovery immediately follows the programming at a heating rate of 3 °C/min, which means that the starting temperature for recovery is different (20 and 40 °C, respectively). It can be seen that a higher T_0 significantly increases the shape fixity ratio due to the decrease of molecular segmental resistance during the plastic flow and shortens the recovery time period. And as the temperature-recovery strain subfigure in Fig. 11(a) shows, the two programmed SMPs generally follow a similar recovery path except for the small deviation caused by the structure relaxation and thermal expansion. For Case (b), the sample programmed at 40 °C is first cooled to 20 °C before being heated to recover, which means that the starting

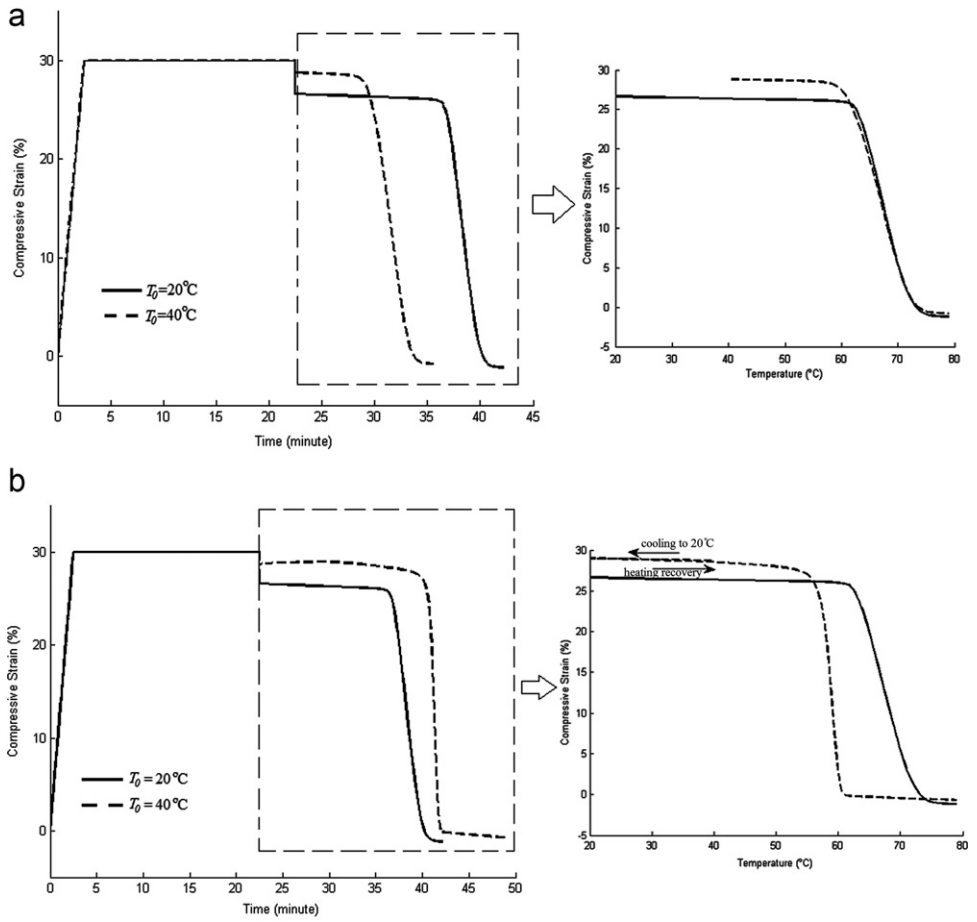

Fig. 11. Thermomechanical cycle results for different programming temperatures: (a) programming followed with immediate heating recovery (b) programming followed with cooling then heating recovery.

temperature for recovery is the same (20 °C). It can be seen from Fig. 11(b) that for the sample programmed at 40 °C, it takes a longer time for completion of Step 4 but with the major recovery completed at a lower temperature, again showing a time–temperature equivalency.

6. Conclusions

The thermomechanical behavior of the thermally responsive thermoset SMP with a unique programming process at glassy temperature has been studied both experimentally and theoretically. The important results of this work include:

(1) The approach of cold-compression programming of a thermosetting shape memory polymer was proposed, tested, and modeled in this study. The test results show that this is an effective and efficient method which achieves very large and durable shape fixity, and has similar shape memory capability to specimens programmed by the lengthy, labor-intensive, and energy-consuming approach currently used.
(2) The concept that the shape memory effect in nature is the transition between equilibrium and nonequilibrium configuration of the SMP structure, which was proposed by Nguyen et al. (2008), can explain the shape memory mechanism of a thermoset SMP programmed by cold-compression.
(3) It is found that the prestrain level must be larger than the yielding strain of the SMP in order to fix a temporary shape at temperatures below T_g.
(4) Longer stress relaxation time leads to larger shape fixity ratio. The upper bound of the shape fixity is determined by the difference between the prestrain and the spring-back which is the ratio of the relaxed stress over the relaxed modulus.
(5) A finite deformation theory and mechanism based thermoviscoelastic constitutive model has been developed to study the thermomechanical behavior of the SMP programmed by cold-compression. Because the pseudo-plasticity and

structure evolution are incorporated, the model reasonably captures the essential characteristics of the shape memory response. A fairly good agreement has been reached between the testing and modeling.

(6) The parametric simulation study reveals that the shape memory behavior is highly dependent on the heating profile. A faster heating rate shifts the onset of the recovery to a higher temperature.

(7) The effect of heating history further corroborates that the shape recovery response turns out to be more of a thermodynamic structure evolution than a steady state variable determined phase transition process. Beyond the glass transition temperature, even without further heating to a higher temperature, an adequate time period of soaking can still help achieve the full recovery.

(8) As long as the programming occurs in glassy state, the programming at a higher temperature followed with an immediate heating recovery leads to a higher shape fixity ratio and has slight effect on the strain recovery. And the recovery of the SMP programmed at a higher temperature followed with a cooling process initiates at a lower temperature and progresses at a faster rate.

(9) It seems that the time–temperature equivalence principle holds for the shape memory behavior. Similar shape recovery ratio can be achieved at a higher temperature with a shorter time period of soaking or a longer time period of soaking at a lower temperature.

Acknowledgments

This work is funded by NSF under grant numbers CMMI 0946740 and CMMI 0900064. The authors also gratefully appreciate the help from Mr. Hari Konka and Dr. Kun Lian for the DMA test.

Appendix A

See Fig. A1 for the flowchart of the MATLAB program.

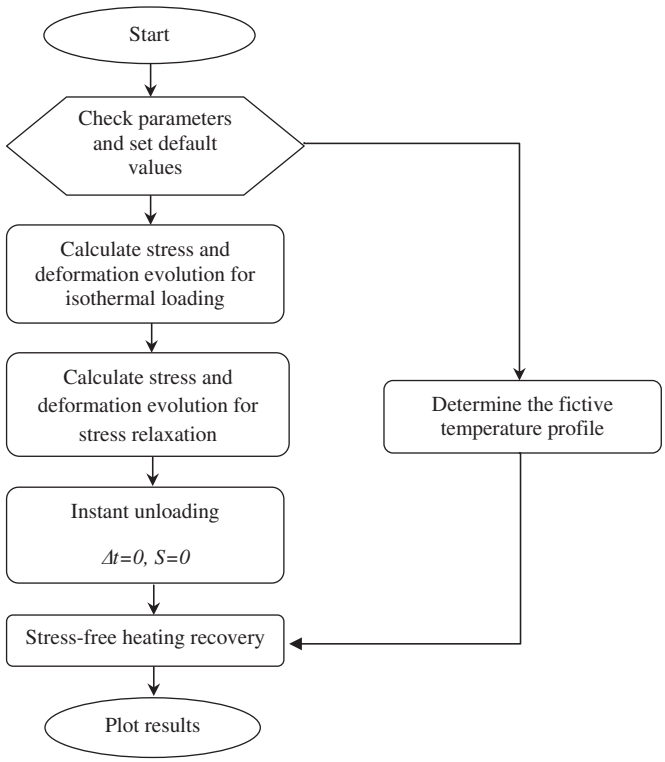

Fig. A1. Flowchart of the MATLAB program.

Appendix B

Although the final values of the material parameters used for demonstration, as listed in Table 2, were mainly obtained from curve fitting various testing results shown in Figs. B1–B4, several basic guidelines were somehow followed to estimate and assist in the initial guesses:

(1) A cooling profile of the thermal deformation is plotted versus the temperature in Fig. B1. The reference height L_0 denotes the initial sample height. It can be observed that the thermal response is not linear as the temperature traverses through the glass transition region. Linear α_r and α_g were computed from the slopes at both above and below the T_g. Volumetric CTEs is three times the values of the linear CTEs.
(2) μ_r and λ_L are the parameters characterizing the rubbery behavior of the material, and can be determined from the stress–strain response at temperatures above T_g (Fig. B2). Lamé constants G and λ can be related to the initial slope of the isothermal

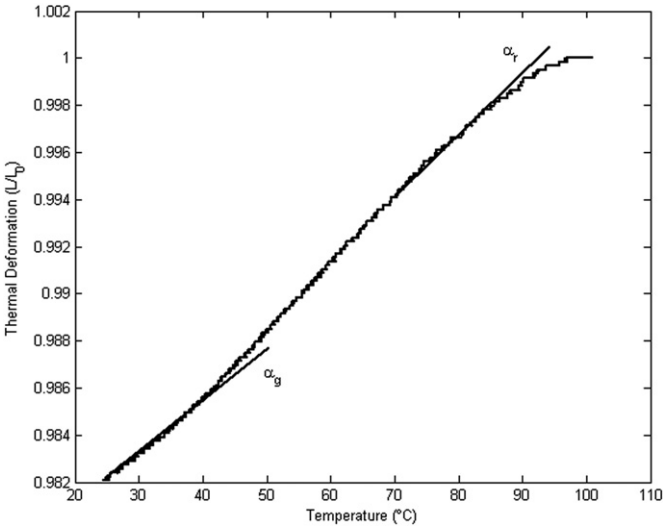

Fig. B1. Thermal response to a stress-free cooling.

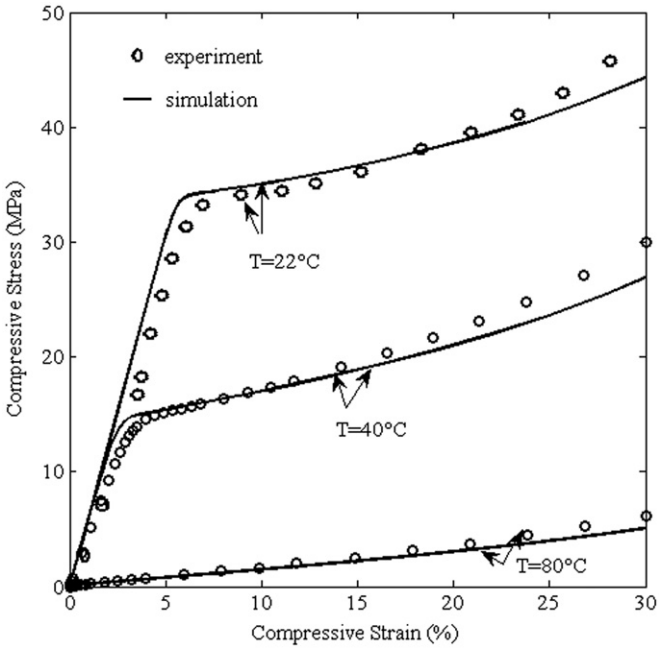

Fig. B2. Stress–strain response of the SMP at different temperatures.

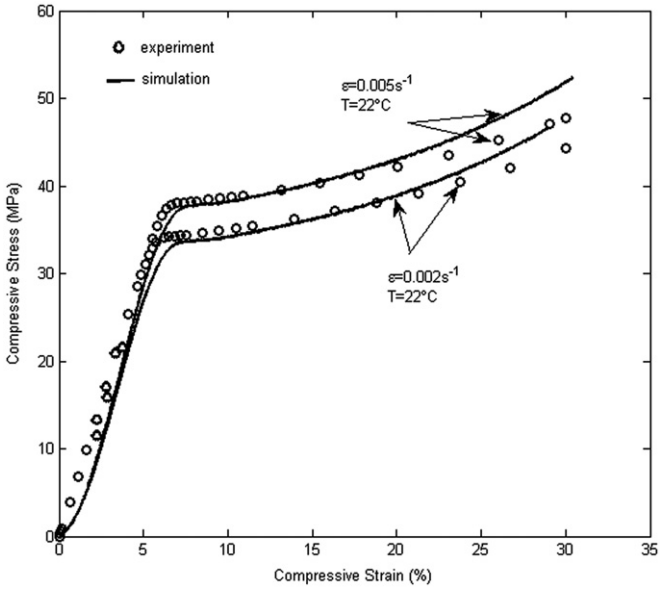

Fig. B3. Stress–strain response of the SMP at different strain rates.

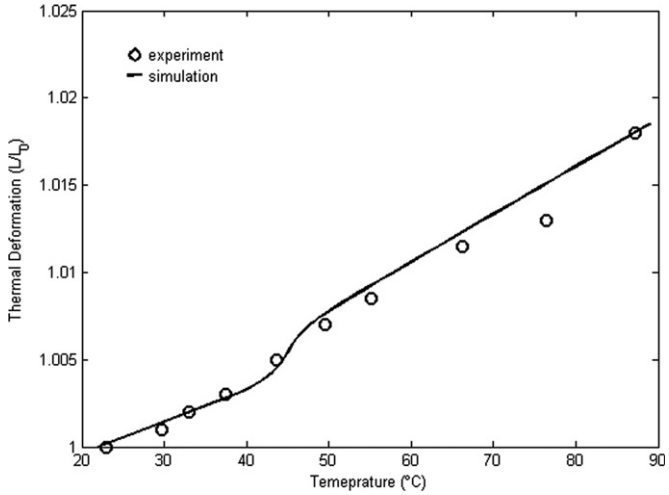

Fig. B4. Thermal response for a stress-free, constant heating rate ($q=0.56$ °C/min) test.

uniaxial compression stress–strain curve in glassy state by assuming a typical polymer Poisson's ratio of 0.4 (Qi et al., 2008). Although it has been suggested that different sets of parameters μ_r and λ_L are preferable to capture the fundamentally different response of the rubbery state and the glassy state (Anand and Ames, 2006; Qi et al., 2008), they are treated to be temperature independent for the sake of convenience in parameter identification and computational simplicity.

(3) As suggested in previous efforts (Boyce et al., 1989; Nguyen et al., 2008; Qi et al., 2008), the viscoplastic parameters such as Q, s, s_s, and h can be roughly determined from the curve fitting of the compression tests at different strain rates (Fig. B3). The ratio Q/s determines the strain rate dependence of the yield strength, and s/s_s indicates the drop of the shear strength. h characterizes the strain-softening rate after yielding.

(4) The structure relaxation parameters x and β are fitted to a stress-free, constant heating profile of the thermal deformation (Fig. B4).

Appendix C

For uniaxial compression, if we consider that the load is applied in the $\mathbf{n}_1$ direction, the mathematical formula can be further reduced as follows:

Because of the assumption of isotropic material and uniform stress field

$$\boldsymbol{F}=\begin{bmatrix}\lambda_1 & & \\ & \lambda_2 & \\ & & \lambda_2\end{bmatrix} \tag{C.1}$$

here λ_1 represents the stretch in $\mathbf{n}_1$ direction and λ_2 is the stretches in the other two directions.

Furthermore, the isochoric left Cauchy strain tensor can be specified as

$$\overline{\boldsymbol{B}}=(J_n)^{-2/3}\begin{bmatrix}\lambda_1^2 & & \\ & \lambda_2^2 & \\ & & \lambda_2^2\end{bmatrix},\quad J_n=\lambda_1(\lambda_2)^2/J_T \tag{C.2}$$

Hence the effective stretch λ_{chain} is defined as

$$\lambda_{chain}=(J_n)^{-1/3}\sqrt{\frac{{\lambda_1}^2+2{\lambda_2}^2}{3}} \tag{C.3}$$

If λ_1^e and λ_2^e denote the elastic stretches, $J_e=\lambda_1^e(\lambda_2^e)^2$. Then the equilibrium and the nonequilibrium stresses can be identified by

$$\boldsymbol{\sigma}_n=\frac{{\lambda_1}^2-{\lambda_2}^2}{3{J_n}^{5/3}}\mu_r\frac{\lambda_L}{\lambda_{chain}}\mathcal{L}^{-1}\left(\frac{\lambda_{chain}}{\lambda_L}\right)\begin{bmatrix}2 & & \\ & -1 & \\ & & -1\end{bmatrix}+k_b(J-1)\boldsymbol{I} \tag{C.4}$$

$$\boldsymbol{\sigma}_{ve}=\frac{1}{J_e}\begin{bmatrix}\ln(\lambda_1^{e(2G+\lambda)}\lambda_2^{e2\lambda}) & & \\ & \ln(\lambda_1^{e\lambda}\lambda_2^{e2(G+\lambda)}) & \\ & & \ln(\lambda_1^{e\lambda}\lambda_2^{e2(G+\lambda)})\end{bmatrix} \tag{C.5}$$

As a result, the equivalent shear stress

$$\overline{\tau}=\frac{2\sqrt{3}}{3J_e}G\left|\ln\frac{\lambda_1^e}{\lambda_2^e}\right|.$$

References

Anand, L., Ames, N.M., 2006. On modeling the micro-indentation response of amorphous polymer. Int. J. Plasticity 22, 1123–1170.

Arruda, E.M., Boyce, M.C., 1993. A three-dimensional constitutive model for the large stretch behavior of rubber elastic materials. J. Mech. Phys. Solids 41, 389–412.

Behl, M., Lendlein, A., 2007. Shape-memoy polymers. Mater. Today 10 (4), 20–28.

Bergstrom, J.S., Boyce, M.C., 1998. Constitutive modeling of the large strain time-dependence behavior of elastomers. J. Mech. Phys. Solids 46 (5), 931–954.

Bhattacharyya, A., Tobushi, H., 2000. Analysis of the isothermal mechanical response of a shape memory polymer rheological model. Polym. Eng. Sci. 40 (12), 2498–2510.

Boyce, M.C., Parks, D.M., Argon, A.S., 1988a. Large inelastic deformation of glassy-polymers. 1: rate dependent constitutive model. Mech. Mater. 7 (1), 15–33.

Boyce, M.C., Park, D.M., Argon, A.S., 1988b. Large inelastic deformation of glassy-polymers. 2: numerical-simulation of hydrostatic extrusion. Mech. Mater. 7 (1), 35–47.

Boyce, M.C., Weber, G.G., Parks, D.M., 1989. On the kinematics of finite strain plasticity. J. Mech. Phys. Solids 37 (5), 647–665.

Boyce, M.C., Kear, K., Socrate, S., Shaw, K., 2001. Deformation of thermoplastic vulcanizates. J. Mech. Phys. Solids 49 (5), 1073–1098.

Chen, Y.H., Lagoudas, D.C., 2008a. A constitutive theory for shape memory polymers. Part I—large deformations. J. Mech. Phys. Solids 56, 1752–1765.

Chen, Y.H., Lagoudas, D.C., 2008b. A constitutive theory for shape memory polymers. Part II—a linearized model for small deformations. J. Mech. Phys. Solids 56, 1766–1778.

Diani, J., Gall, K., 2007. Molecular dynamics simulations of the shape-memory behaviour of polyisoprene. Smart Mater. Struct. 16, 1575–1583.

Donth, E., Hempel, E., 2002. Structural relaxation above the glass temperature: pulse response simulation with the Narayanaswamy Moynihan model for glass transition. J. Non-Cryst. Solids 306, 76–89.

Eyring, H., 1936. Viscosity, plasticity, and diffusion as examples of absolute reaction rates. J. Comput. Phys. 28, 373–383.

Flory, P.J., 1961. Thermodynamic relations for highly elastic materials. Trans. Faraday Soc. 57, 829–838.

Gall, K., Yakacki, C.M., Liu, Y., Shandas, R., Willett, N., Anseth, K.S., 2005. Thermomechanics of the shape memory effect in polymers for biomedical applications. J. Biomed. Mater. Res. A 73, 339–348.

Govindjee, S., Reese, S., 1997. A presentation and comparison of two large deformation viscoelasticity models. Trans. ASME J. Eng. Mater. Technol. 119, 251–255.

Govindjee, S., Simo, J., 1991. A micro-mechanically based continuum damage model for carbon black-filled rubbers incorporating Mullins effect. J. Mech. Phys. Solids 39 (1), 87–112.

Hempel, E., Kahle, S., Unger, R., Donth, E., 1999. Systematic calorimetric study of glass transition in the homologous series of poly(n-alkyl methacrylate)s: Narayanaswamy parameters in the crossover region. Thermochim. Acta 329, 97–108.

John, M., Li, G., 2010. Self-healing of sandwich structures with a grid stiffened shape memory polymer syntactic foam core. Smart Mater. Struct. 19 (7), 1–12 (paper number 075013).

Kafka, V., 2001. Mesomechanical Constitutive Modeling. World Scientific, Singapore.

Kafka, V., 2008. Shape memory polymers: a mesoscale model of the internal mechanism leading to the SM phenomena. Int. J. Plast. 24, 1533–1548.
Kohlrausch, F., 1847. Pogg. Ann. Phys. 12, 393–399.
Lendlein, A., Langer, R., 2002. Shape memory polymers. Angew. Chem. Int. Ed. 41, 2034–2057.
Lendlein, A.S., Kelch, S., Kratz, K., Schulte, J., 2005. Shape-memory polymers. In: Bhattacharya, K. (Ed.), Encyclopedia of Materials. Elsevier, Amsterdam.
Li, G., John, M., 2008. A self-healing smart syntactic foam under multiple impacts. Compos. Sci. Technol. 68 (15–16), 3337–3343.
Li, G., Nettles, D., 2010. Thermomechanical characterization of a shape memory polymer based self-repairing syntactic foam. Polymer 51 (3), 755–762.
Li, G., Uppu, N., 2010. Shape memory polymer based self-healing syntactic foam: 3-D confined thermomechanical characterization. Comp. Sci. Technol. 40 (9), 1419–1427.
Lion, A., 1997. On the large deformation behavior of reinforced rubber at different temperatures. J. Mech. Phys. Solids 45, 1805–1834.
Liu, Y.P., Gall, K., Dunn, M.L., McCluskey, P., 2004. Thermomechanics of shape memory polymer nanocomposites. Mech. Mater. 36 (10), 929–940.
Liu, Y., Gall, K., Dunn, M.L., Greenberg, A.R., Diani, J., 2006. Thermomechanics of shape memory polymers: uniaxial experiments and constitutive modeling. Int. J. Plast. 22, 279–313.
Lu, S.C.H., Pister, K.S., 1975. Decomposition of deformation and representation of the free energy function for isotropic thermoelastic solids. Int. J. Solids Struct. 11, 927–934.
Miehe, C., Keck, J., 2000. Superimposed finite elastic–viscoelastic–plastoelastic stress response with damage in filled rubbery polymers. Experiments, modelling and algorithmic implementation. J. Mech. Phys. Solids 48 (2), 323–365.
Morshedian, J., Khonakdar, H.A., Rasouli, S., 2005. Modeling of shape memory induction and recovery in heatshrinkable polymer. Macromol. Theory Simulat. 14, 428–434.
Moynihan, C.T., Easteal, A.E., Debolt, M.A., Tucker, J., 1976. J. Am. Ceram. Soc. 59, 12–16.
Nakayama, K., 1991. Properties and application of shape-memory polymers. Int. J. Polym. Sci. Technol. 19, T43–T48.
Narayanaswamy, O.S., 1971. A model of structural relaxation in glass. J. Am. Ceram. Soc. 54 (10), 491–498.
Nguyen, T.D., Qi, H., Castro, F., Long, K.N., 2008. A thermoviscoelastic model for amorphous shape memory polymers: incorporating structural and stress relaxation. J. Mech. Phys. Solids 56 (9), 2792–2814.
Nji, J., Li, G., 2010a. A self-healing 3D woven fabric reinforced shape memory polymer composite for impact mitigation. Smart Mater. Struct. 19 (3), 1–9 (paper number 075013).
Nji, J., Li, G., 2010b. A biomimic shape memory polymer based self-healing particulate composite. Polymer 51, 6021–6029.
Otsuka, K., Wayman, C.M., 1998. Shape Memory Materials. Cambridge University Press, New York.
Qi, H.J., Boyce, M.C., 2005. Stress–strain behavior of thermoplastic polyurethanes. Mech. Mater. 37 (8), 817–839.
Qi, H.J., Nguyen, T.D., Castro, F., Yakacki, C.M., Shandas, R., 2008. Finite deformation thermo-mechanical behavior of thermally induced shape memory polymers. J. Mech. Phys. Solids 56, 1730–1751.
Ping, P., Wang, W., Chen, X., Jing, X., 2005. Poly(ε-caprolactone) polyurethane and its shape-memory property. Biomacromolecules 6, 587–592.
Rabani, G., Luftmann, H., Kraft, A., 2006. Synthesis and characterization of two shape-memory polymers containing short aramid hard segaments and poly(ε-caprolactone) soft segments. Polymer 47, 4251–4260.
Scherer, G.W., 1990. Theories of relaxation. J. Non-Cryst. Solids 123, 75–89.
Sidoroff, F., 1974. Un modèle viscoélastique non linéaire avec configuration intermédiare. J. Mec. 13, 679–713.
Simo, J.C., Taylor, R.L., Pister, K.S., 1985. Variational and projection methods for the volume constraint in finite deformation elasto-plasticity. Comput. Methods Appl. Mech. Eng. 51, 177–208.
Tobushi, H., Hara, H., Yamada, E., Hayashi, S., 1996. Thermomechanical properties in a thin film of shape memory polymer of polyurethane series. Smart Mater. Struct. 5 (4), 483–491.
Tobushi, H., Hashimoto, T., Hayashi, S., Yamada, E., 1997. Thermomechanical constitutive modeling in shape memory polymer of polyurethane series. J. Intell. Mater. Syst. Struct. 8, 711–718.
Tool, A.Q., 1946. Relation between inelastic deformability and thermal expansion of glass in its annealing range. J. Amer. Ceram. Soc. 29 (9), 240–253.
Treloar, L.R.G., 1958. The Physics of Rubber Elasticity. Clarendon Press, Oxford.
Wang, W., Jin, Y., Ping, P., Chen, X., Jing, X., Su, Z., 2010. Structure evolution in segmented poly(ester urethane) in shape-memory process. Macromolecules 43, 2942–2947.
William, M.L., Landel, R.F., Ferry, J.D., 1955. The temperature dependence of relaxation mechanisms in amorphous polymers and other glass-forming liquids. J. Amer. Chem. Soc. 77, 3701–3707.
Xu, W., Li, G., 2010. Constitutive modeling of shape memory polymer based self-healing syntactic foam. Int. J. Solids Structs. 47 (9), 1306–1316.
Yakacki, C.M., Shandas, R., Lanning, C., Rech, B., Eckstein, A., Gall, K., 2007. Unconstrained recovery characterization of shape-memory polymer networks for cardiovascular applications. Biomaterials 28 (14), 2255–2263.
Zotzmann, J., Behl, M., Feng, Y., Lendlein, A., 2010. Copolymer networks based on poly(ω-pentadecalactone) and poly(ε-caprolactone) segments as a versatile triple-shape polymer system. Adv. Funct. Mater. 20, 3583–3594.